# ACT2: a High Heat Flux Test Facility Using Electron Beam for Fusion Application*)

Yukinori HAMAJI, Masayuki TOKITANI, Suguru MASUZAKI, Ryuichi SAKAMOTO, Hitoshi TAMURA and Akio SAGARA

*National Institute for Fusion Science, 322-6 Oroshi-cho, Toki 509-5292, Japan*

(Received 30 November 2015 / Accepted 26 January 2016)

ACT2 (Active Cooling Teststand 2), a high heat flux test facility using electron beam has been upgraded from ACT facility and started the operation. A new electron gun enables the steady state and transient heat load on actively cooled samples. ACT2 can achieve large loaded area with steady state reactor relevant heat flux ($\sim 20\,\mathrm{MW/m^2}$) up to $200 \times 200\,\mathrm{mm^2}$ and simulation of edge localized modes with short pulse length ($\sim 100\,\mu\mathrm{s}$). Beam profile was obtained about 9 mm with graphite probes. The heat flux is obtained by water calorimetry and measurement of the current through the samples.



Keywords: plasma facing component, divertor, heat flux, edge localized mode, fatigue, electron beam, heat removal, active cooling

DOI: 10.1585/pfr.11.2405089

## 1. Introduction

Plasma facing components (PFCs) will be subjected to severe high heat flux in DEMO and beyond. PFCs must satisfy requirements such as: high heat removal capability, reliability, long fatigue lifetime and endurance against thermal shocks. To confirm the performance of PFCs against the severe heat flux, heat flux tests with reactor relevant heat flux are necessary for the R&D activities of PFCs. Electron beam is widely used for high heat flux test facilities [1–5]. Electron beam was relatively easy to scan desired area and control input power and the density compared with other methods.

ACT2 (Active Cooling Teststand 2), a high heat flux test facility, has been upgraded from ACT facility [6]. ACT2 facility was built in the National Institute for Fusion Science, Japan. ACT2 is designated for heat flux tests of PFCs of DEMO and beyond such as FFHR-d1 [7] and research activities of material response against transient heat flux such as edge localized modes (ELMs). In this paper, we make an introduction of ACT2 facility. Characteristics of ACT2's electron gun, control system, employed components, data acquisition system, heat flux calculation from current and examples of actual operations of ACT2 were shown.

## 2. Properties of ACT2 Facility

### 2.1 Electron gun

An electron gun control system, JEBG-3000UB manufactured by JEOL Ltd. is equipped on ACT2. The system includes power supplies, electron gun, deflection lenses and vacuum system for the gun. This electron gun uses thermal cathode to generate the electron beam. Table 1 shows the characteristics of ACT2 facility. The maximum power of the electron gun is 300 kW. Focused beam can be scanned by deflection lenses with deflection angle up to 60 degree. However, achievable heated area in ACT2 is limited by its vacuum chamber. The maximum heated area of ACT2 is $500 \times 500$ mm. Start-up of the beam and changing the beam power takes over one minute typically. ACT2 can scan rectangle areas with decided frequency. User defines a center coordination and width of the target area in $x$ and $y$ direction. Up to 10 points can be defined for scans with each coordination, scanning width and dwell time. Therefore, cyclic heat flux test can be performed fully automatically. Minimum dwell time for a point is practically about several tens micro seconds. Spot size of ACT2's beam is about 9 mm in FWHM (discussed in the next section). Due to this relatively large spot size, it's easy to avoid to make un-irradiated area and reduce local peak heat flux compared with other facilities with highly focused beam. On the other hand, the beam spot size causes inhomogeneous heating at the edge of the target area. To eliminate the edge effect, a water cooled beam dump with a particular aperture located right above the sample is employed. The location of the beam dump is shown in Fig. 1. Designated beam dump is required for each target area.

The tested sample is insulated from the chamber. The current of incident electron is discharged to ground through a resistor. During experiment, heat flux is monitored as the current through the resistor in real time. There are two types of data acquisition path using the same resistor. One is using high speed digitizer with 1 μs sampling rate. This digitizer is enough fast to observe 5 kHz scanning of the

*author's e-mail: hamaji.yukinori@nifs.ac.jp*

*) This article is based on the presentation at the 25th International Toki Conference (ITC25).

Table 1 Technical Characteristics of ACT2.

| *Parameter* | Value | unit |
|---|---|---|
| *Max. beam power* | 300 | kW |
| *Accelerating voltage* | 40 | kV DC |
| *Max. beam current* | 7.5 | A |
| *Beam deflection frequency in x direction* | 500 | Hz |
| *Beam deflection frequency in y direction* | 5000 | Hz |
| *Max. heated Area (limited by the vacuum chamber)* | 500 × 500 | mm |
| *Beam spot diameter (FWHM)* | ~9 | mm |
| *Typical flow rate of the cooling water* | 42 | l/min. |

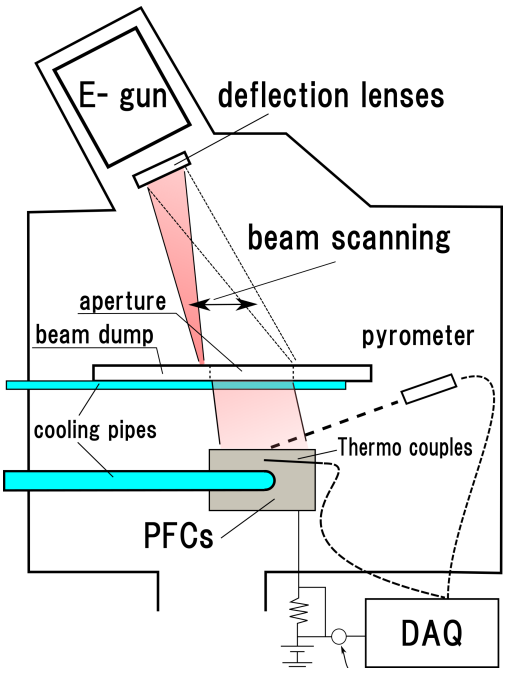


Fig. 1 Schematic view of ACT2 facility.

beam. However, there is a limitation of maximum amount of samples for one measurement. Therefore, the digitizer is used only for short measurements such as transient load or detailed observation of beam scanning. For longer experiments, another digitizer with lower sampling rate (0.2 seconds) is used. The slower digitizer enables to monitor long-term heat flux in real time. In this data acquisition path, isolated amplifier using photocoupler is employed to average the current through the sample to eliminate the effects of high frequency components of the current through the sample.

## 2.2 Beam profile

Beam profile was measured using two insulated graphite probes set on a graphite tile. The two probes with hemispherical head of 2 mm in diameter are located 30 mm apart. The probes obtained current signals of the beam scanned over the probes. The beam profile was obtained by scanning speed and current through a probe. A typical beam profile is shown in Fig. 2. I note that the diameter of probe is not enough narrow to obtain detailed profile

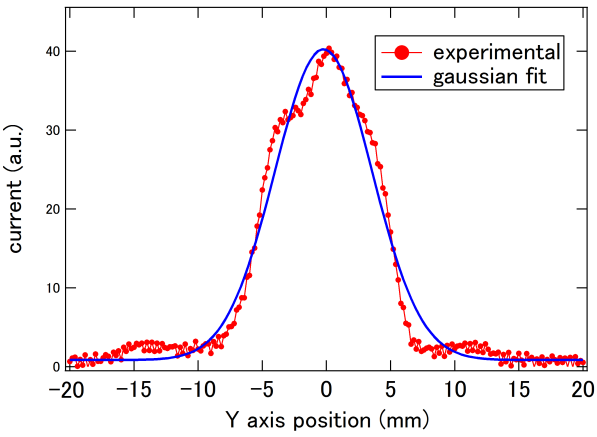


Fig. 2 Beam profile of ACT2's electron beam measured by probe. A probe signal is shown as red line with circle symbol. Blue line indicates the result of the Gaussian fitting.

because this probe needs enough heat capacity.

## 2.3 Heat load calculation from the current

Absorbed heat load on sample can be measured by water calorimetry. It's accurate and simple. However, the latency and error in case of lower heat load are significant. Current measurement has good properties in this aspect. It is very fast, sensitive for change of beam power and not depend on heat load.

During irradiation, a part of incident electron do not contribute on current because of reflection. However, reflected electrons also deposit some part of their energy on the sample because the collisions between electrons and material's atoms are inelastic. Therefore, energy deposition by reflected electron have to be considered. Theoretical descriptions of electron reflection behavior and energy transfer from incident electrons are developed quantitatively [8]. Characteristics of the incident electron depend on not incident energy but atomic number of the material. For instance, based on ref. [8], the effect of reflection on the carbon material is negligible. On the other hand, in case of tungsten, reflection coefficient and the average energy of reflected electrons relative to incident electron energy are about 49 % and 73 % respectively. These values means that the heat load by reflected electron reaches about

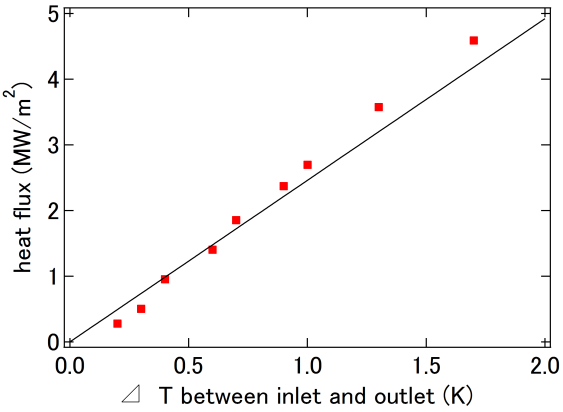


Fig. 3 Comparison between heat flux calculated from measured current through the sample (red squire symbols) and water calorimetry (black line).

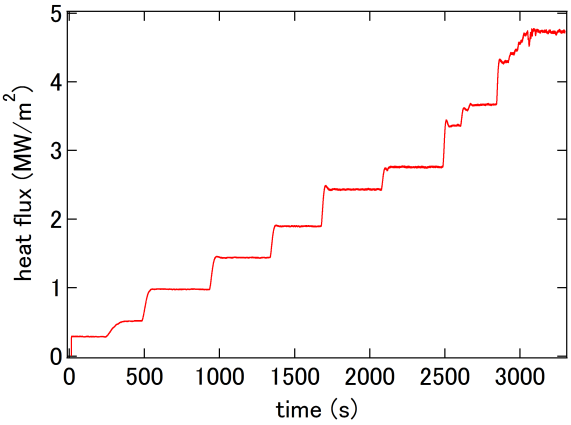


Fig. 4 A example of steady state heat flux test. Ramping up of beam takes over one minute. Turbulences of the beam were observed only in the last part.

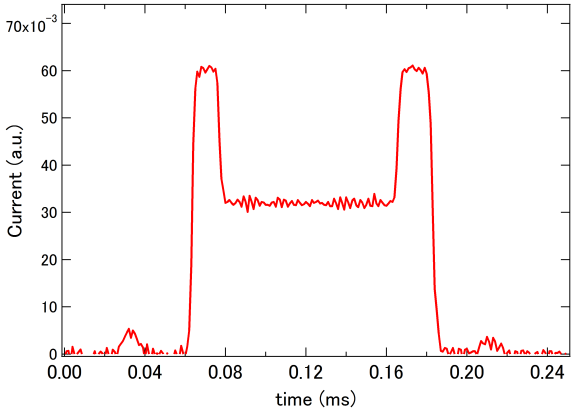


Fig. 5 A short pulse load test. two peaks shows beam transfer duration through on the graphite tile. Actual irradition on the W block is about 80 μs in this case.

one fifth of total heat load on tungsten.

To confirm the contribution of reflected electron, a comparison between heat load calculations discuss above and the results of water calorimetry was performed. Figure 3 shows the results of the comparison. In this experiments a three 20 × 20 × t5 mm W blocks brazed on Cu heat sink was used. The three blocks were arrayed in a row. The flow rate of cooling water for the sample was 42 l/min. The sample was biased to 80 V to recollect the secondly electrons. The bias is not significant for heat load because the voltage was enough small compared with energy of reflected electrons. Homogeneous heating and the heated area 20 × 60 mm was assumed. The solid line in Fig. 3 corresponds to the heat flux calculated from temperature difference between water inlet and outlet. The heat flux calculated from measured current are plotted against the experimental temperature difference in square symbols. In this calculation, radiation was neglected because of low surface temperature estimated from bulk temperature of the sample measured by thermocouples. The results of water calorimetry and the heat flux calculation were agreed.

# 3. Actual Heat Load Test

## 3.1 Steady-state

A steady state heat load on brazed W block described section 2.3 is picked as an example of actual operation of ACT2. Figure 4 shows the heat flux applied on the sample against time. The heat flux was ramped up in stages by changing the output current. This heat flux was from current measured by digitizer with lower sampling rate described section 2.1. The heat flux on each stage shows relatively small ripples except over 4 MW/m$^2$. In the 4 MW/m$^2$ case, the chamber pressure increased by heating up the chamber walls and cooling circuit. To achieve heat flux test with higher heat flux, we will modify of the chamber cooling system and replace the tubing of cooling water.

## 3.2 Transient load

Transient heat load test is also available in ACT2 facility. Structure of cracks on the W surface induced by transient load is typically less than sub mm scale [9–12]. The spot size of ACT2's electron beam is larger than the scale. Therefore, material responses to transient load can be investigated in simple irradiation condition without scanning. In practical, ACT2's beam system can control irradiation position in the order of 100 μs. This is enough short to simulate ELMs. However, in this time scale, the duration of beam transfer between the beam dump and irradiation position is not negligible. ACT2's beam monitoring system cannot observe actual beam position. Therefore, to evaluate the duration of beam transfer, we performed a designated experiment. In the experiment, the beam scanned on the beam dump then irradiated W block (50 × 50 × t5 mm) put on a graphite tile, then backed to the beam dump. Distance between the edge of beam dump and the center of W block is 100 mm. As I mentioned in section 2.3, reflection coefficients on graphite and tungsten are different. Therefore, we can obtain the duration

of beam transfer between the beam dump and W block by measuring current through them. Figure 5 shows the current through graphite or W. irradiation dwell time on the W block was set for 100 μs. In this case, beam transfer took over 10 μs and actual irradiation time is about 80 μs. This speed of beam transfer obtained here is applicable only for this geometry because the speed should be depend on the transfer angle. However, transient load with accurate irradiation time is achievable using this kind of experiments.

# 4. Summary

ACT2 (Active Cooling Teststand 2), a high heat flux test facility started its operation. ACT2 is a upgraded facility using electron beam from ACT facility. A newly installed electron gun and data acquisition systems of ACT2 enables powerful and flexible experiments for R&D activities of plasma facing components (PFCs) for DEMO and beyond.

In this paper, technical characteristics of ACT2 facility are introduced. Focused electron beam scans defined area using high frequency deflection lenses. 300 kW beam power and 60 degree of deflection angle of ACT2's electron gun allow to apply reactor relevant heat flux into defined area. Two data acquisition system with high sampling rate and low sampling rate were prepared for both of steady state and transient heat load. The spot size of the electron beam about 9 mm in diameter was measured using graphite probes. A calculation of heat load from current through sample was employed for fast and real-time monitoring of heat load. The calculation of heat flux agreed with the result of water calorimetry due to consider the contribution of reflected electron on heat load. The actual operation of steady-state and transient load were shown. In transient heat load test, the transfer time of beam was considered to define the heat load duration.


[1] P. Majerus, R. Duwe, T. Hirai, W. Kühnlein, J. Linke and M. Rödig, Fusion Eng. Des. **75-79**, 365 (2005).

[2] I. Bobin-Vastra, F. Escourbiac, M. Merola and P. Lorenzetto, Fusion Eng. Des. **75-79**, 357 (2005).

[3] D.L. Youchison, J.M. Mcdonald, L.S. Wold, R.D. Boyd and A.J. Ghajar, Heat Transf. High Heat Flux Syst. ASME B. No. G00956, Am. Soc. Mech. Eng. (ASME), (1994).

[4] V. Kuznetsov, A. Gorbenko, V. Davydov, A. Kokoulin, A. Komarov, I. Mazul, B. Mudyugin, I. Ovchinnikov, N. Stepanov, R. Rulev and A. Volodin, Fusion Eng. Des. **89**, 955 (2014).

[5] M. Akiba, M. Araki, S. Suzuki, S. Tanaka, M. Dairaku, K. Yokoyama and M. Seki, Plasma Devices Oper. **1**, 205 (1991).

[6] Y. Kubota, N. Noda, A. Sagara, R. Sakamoto, O. Motojima, I. Fujita, T. Hino, T. Yamashina, K. Tokunaga and N. Yoshida, Fusion Eng. Des. **39-40**, 247 (1998).

[7] A. Sagara, H. Tamura, T. Tanaka, N. Yanagi, J. Miyazawa, T. Goto, R. Sakamoto, J. Yagi, T. Watanabe and S. Takayama, Fusion Eng. Des. **89**, 2114 (2014).

[8] I.S. Tilinin, Phys. Chem. Mech. Surfaces **5**, 476 (1989).

[9] M. Wirtz, G. Cempura, J. Linke, G. Pintsuk and I. Uytdenhouwen, Fusion Eng. Des. **88**, 1768 (2013).

[10] Y. Kikuchi, I. Sakuma, D. Iwamoto, Y. Kitagawa, N. Fukumoto, M. Nagata and Y. Ueda, J. Nucl. Mater. **438**, S715 (2013).

[11] T. Loewenhoff, A. Bürger, J. Linke, G. Pintsuk, A. Schmidt, L. Singheiser and C. Thomser, Phys. Scr. **T145**, 014057 (2011).

[12] A. Huber, A. Arakcheev, G. Sergienko, I. Steudel, M. Wirtz, A.V. Burdakov, J.W. Coenen, A. Kreter, J. Linke, P. Mertens, V. Philipps, G. Pintsuk, M. Reinhart, U. Samm, A. Shoshin, B. Schweer, B. Unterberg and M. Zlobinski, Phys. Scr. **T159**, 014005 (2014).